REPORT DOCUMENTATION PAGE

AFRL-SR-AR-TR-05-

0038

1. REPORT DATE (DD-MM-YYYY)	2. REPORT TYPE	3. DATES COVERED (From - To)
January 31, 2005	Final Performance	9/1/2001-8/31/2004

4. TITLE AND SUBTITLE

Bio-Derived Photonic Assemblies

5a. CONTRACT NUMBER
F49620-01-1-0509

5b. GRANT NUMBER

5c. PROGRAM ELEMENT NUMBER

6. AUTHOR(S)

Thomas, Edwin L., Morris Cohen Professor of Materials Science and Engineering

Mickiewicz, Rafal

5d. PROJECT NUMBER

5e. TASK NUMBER

5f. WORK UNIT NUMBER

7. PERFORMING ORGANIZATION NAME(S) AND ADDRESS(ES)

Prof. Edwin L. Thomas
Massachusetts Institute of Technology
77 Massachusetts Avenue
Room 13-5094
Cambridge, MA 02139

8. PERFORMING ORGANIZATION REPORT NUMBER

9. SPONSORING / MONITORING AGENCY NAME(S) AND ADDRESS(ES)

Dr. Charles Lee
Air Force Aerospace Research-OSR
4015 Wilson Blvd.,Room 713
Arlington, VA 22203-1954

10. SPONSOR/MONITOR'S ACRONYM(S)
AFOSR

11. SPONSOR/MONITOR'S REPORT NUMBER(S)

12. DISTRIBUTION / AVAILABILITY STATEMENT

No Restrictions Approve for Public Release: Distribution Unlimited

13. SUPPLEMENTARY NOTES
None

14. ABSTRACT

Biologically derived photonic assemblies were created using two different approaches. The first method employed the periodic, bi-continuous exoskeleton structure of a sea urchin as a template for the construction of a 3-dimensional (3-D) photonic crystal. The second approach involved viral particles of the *Wiseana* iridescent virus (WIV), assembled by various means to produce colloidal photonic crystals. In the first case, a novel cyclic size reduction scheme was devised to shrink the native sea urchin skeleton structure to the relevant size scale. This method produced high fidelity replicas of the original structure with a 50% decrease in linear dimensions at each iteration. The silicon oxycarbide (SiOC):air replica was subsequently infiltrated with tellurium (Te) and etched to increase the dielectric contrast, resulting in a Te:air structure exhibiting a sharp, well defined reflectivity peak in the mid-IR range. In the second case, sedimentation, centrifugation, and flow-assisted assembly were successfully used to guide virus particles into ordered colloidal crystals with photonic properties in the visible range. The centrifugation and flow-assisted techniques created larger area crystals with better defined spectral properties than the sedimentation technique. Significantly, the spectral properties (color) of both disordered and polycrystalline assemblies could be tuned by swelling the cross-linked colloidal crystals with water and varying processing parameters.

15. SUBJECT TERMS

16. SECURITY CLASSIFICATION OF:			17. LIMITATION OF ABSTRACT	18. NUMBER OF PAGES	19a. NAME OF RESPONSIBLE PERSON
a. REPORT	b. ABSTRACT	c. THIS PAGE			E.L. Thomas
U	U	U	UU	20	19b. TELEPHONE NUMBER (include area code) 617/253-6901

MIT Final Performance Report
Contract # F49620-01-1-0509
Title: Bio-Derived Photonic Assemblies

Principal Investigator:	Prof. Edwin L. Thomas
Phone:	617-253-5931
FAX:	617-253-5859
Mailing Address:	Massachusetts Institute of Technology 77 Massachusetts Avenue, 13-5098 Cambridge, MA 02139
E-Mail Address:	elt@mit.edu

AFOSR Program Manager: Dr. Charles Y-C. Lee

Abstract

Biologically derived photonic assemblies were created using two different approaches. The first method employed the periodic, bi-continuous exoskeleton structure of a sea urchin as a template for the construction of a 3-dimensional (3-D) photonic crystal. The second approach involved viral particles of the *Wiseana* iridescent virus (WIV), assembled by various means to produce colloidal photonic crystals. In the first case, a novel cyclic size reduction scheme, through infiltration and pyrolysis, was devised to shrink the native sea urchin skeleton structure to the relevant size scale. This method produced high fidelity replicas of the original structure with a 50% decrease in linear dimensions at each step and was used to bring the length scale down to the mid-IR range. The silicon oxycarbide (SiOC):air replica was subsequently infiltrated with tellurium (Te) to increase the dielectric contrast. After etching of the SiOC, the resulting Te:air structure exhibited a sharp, well defined reflectivity peak in the mid-IR range. In the second case, sedimentation, centrifugation, and flow-assisted assembly were used to guide virus particles into ordered colloidal crystals. All three techniques were successfully used to create photonic crystals in the visible range. The centrifugation and flow-assisted techniques created larger area crystals with better defined spectral properties than the sedimentation technique. Significantly, the spectral properties (color) of both disordered and polycrystalline assemblies could be tuned by swelling the cross-linked colloidal crystals with water.

Introduction

Significant advances in photonic materials are critical for numerous future Air Force systems, such as Sensor Craft and Space Based Radar. Additionally, Air Force interests in signature control would be positively impacted by the availability of advanced photonic materials suitable for various wavelengths. In contrast to the classical perception of photonics as a component within a discrete telecom device, these future applications require materials organization that is amenable to large-scale integration on flexible substrates, tunable optical properties, and robust mechanical and thermal performance. Photonic band gap structures provide enticing platforms to combine large-scale processablity, a classical motivation driving polymer use, with enhanced photonic properties via exploitation of spatially-defined and locally enhanced optical fields. To date, most emphasis has been on multilayered 1-D,

triangular lattice 2-D, and cubic 3-D structures. These previous studies have barely scratched the surface of the multitude of possible structures and material properties that might be exploited, but have been limited by the complexity associated with fabrication of these more complex structures.

In light of this, the aim of this research was to develop techniques to manipulate naturally occurring periodic materials into mechanically robust, photonic crystal systems possessing 3-D band structures that cannot be obtained through traditional methods. Through evolution, Nature has devised ways to create highly ordered periodic structures with a near perfect level of organization and reproducibility. The goal is to tap into these biologically assembled periodic structures to build systems of practical use. Two general approaches were examined: 1) top-down fabrication based on size reduction of micron-scale periodic structures, such as those found in sea urchin skeletons, and 2) bottom-up fabrication based on assembly of viral particles, such as the iridescent virus. In addition, the investigated processing and fabrication techniques could potentially be integrated with conventional microfabrication technologies to optimize the possibility for integrated optic devices.

Many naturally occurring solids possess periodic structures that give rise to visible photonic crystal properties, commonly termed structural colors. Some stunning examples are butterfly wings, abalone shells, sea mouse spines, and natural opals. These biomaterials can be used as scaffolds and templates to construct photonic crystals with structures that are difficult or impossible to fabricate by artificial means. The scientific literature is replete with examples of biological self-assembled structures that produce iridescent optical effects. Two general areas are being explored within this field: *bio-templates* and *bio-colloids* (essentially top-down and bottom-up approaches to photonic crystals, respectively). Bio-templates refer to natural microstructures that can serve as templates to create multi-scale, multi-component photonic crystals through iterative meso-/micro-molding and casting. Bio-colloids, such as viruses, refer to the utilization of highly structured and complex discrete particles that can be organized into non-FCC arrays via surface directed assembly. For this task, the sea urchin skeleton (*cidaris cidaris*), which exhibits a bicontinuous Schwarz's P-surface structure, was used as the bio-template, whereas the *Wiseana* iridescent virus (WIV) was used as the bio-colloidal building block. Each approach, with the associated techniques developed to create the photonic structures, is described separately in detail in the following sections.

Bio-templates: Top-down Engineering of the Sea Urchin Skeleton

Many naturally occurring solids possess periodic structures that give rise to visible photonic crystal properties, commonly termed structural colors. Exploitation of other periodic natural structures for visible optical applications, however, is limited by the inherently large size scale and the low dielectric contrast of the materials. Furthermore, these generally more complex geometries are a challenge to correctly model in order to obtain correct band diagrams. In this study we used a sea urchin exoskeleton for the successful fabrication of a high dielectric contrast, 3-D photonic crystal exhibiting a stop band in the mid-IR range, through a novel cyclic size reduction and infiltration process. To model the bandgap and the reflectivity of the structure we used level set mathematics to describe the 3-D bicontinuous network of the sea urchin. As mentioned in the introduction, a naturally occurring bicontinuous structure is found the sea urchin exoskeleton (termed stereom). These stereoms are comprised of interpenetrating magnesium calcite ($MgCO_3$) and soft tissue, with periodic spacings typically on the order of a few tens of microns. For this study we used a stereom from the *Phyllacanthus* species interambulacral plates, having a unit cell with a lattice parameter of approximately 30 microns (Figure 1a).

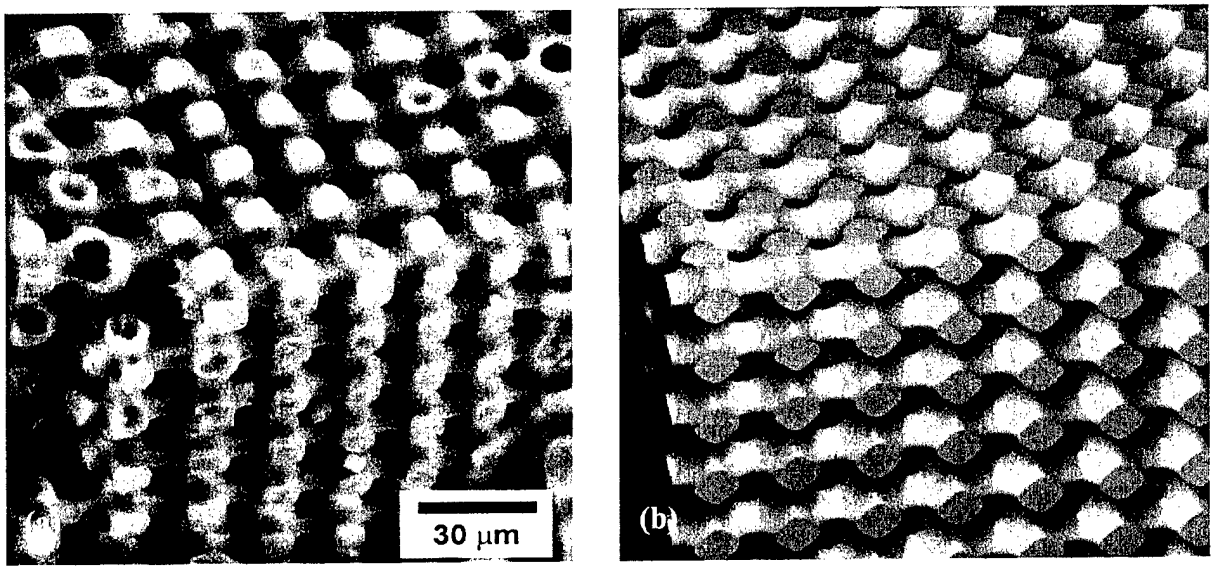

Figure 1. (a) SEM image of a templated structure of the rectilinear stereom from the interambulacral plates of the sea urchin *Phyllacanthus*. After one pyrolysis step, the sample shown consists of a polystyrene:air network. (b) A computer generated level set of the Schwarz's P-surface with a 50 vol% network.

A perfectly periodic, rectilinear stereom may be approximated using a level set equation for Schwarz's P-surface family:

$$10(\cos x + \cos y + \cos z) - 5.1(\cos x \cos y + \cos y \cos z + \cos z \cos x) = t \qquad (1)$$

The structure has cubic $Pm\bar{3}m$ symmetry, where each node has 6 arms directed outwards along the three orthogonal directions. Varying the magnitude of t dilates or contracts the thickness of the arms defining the dividing surface and thus the network volume fraction of the bicontinuous structure. Calculations based on confocal microscopy and comparisons of scanning electron microscope (SEM) area projection with the level set equations give an estimated volume fraction of approximately 50% for the stereom from the *Phyllacanthus* interambulacral plates. A computer-generated 50% network structure is shown in Figure 1b, in a corresponding view to the templated stereom structure.

Using the level set function of Equation 1, we explored several P-surface family members and found that a complete 3-D bandgap opens between the 5^{th} – 6^{th} bands when the dielectric contrast is greater than 8.9:1 at 19% network volume fraction. With increasing dielectric contrast, a second complete bandgap appears between the 2^{nd} – 3^{rd} bands (see supplementary information). Regardless of the dielectric contrast, only a partial gap between the 5^{th} – 6^{th} bands occurs for the 50% volume structure. The native sea urchin structure does not exhibit desirable photonic behaviour due to the low dielectric contrast of magnesium calcite-air structure and the significant absorption of calcite in the mid- and far-IR range.

In order to access the mid-IR reflectivity and to obtain a high dielectric contrast structure with low absorption in the IR, a cyclic isomorphic size reduction scheme followed by a hot-isostatic infiltration step with a semi-metal (tellurium) was devised. Our process starts by filling the sea urchin exoskeleton with a poly(dimethyl siloxane) (PDMS) elastomer. The PDMS is inert to the subsequent HCl etching of the calcite network, thereby creating an inverted-urchin replica. Size reduction occurs during the pyrolysis of the PDMS into silicon oxycarbide (SiOC), which uniformly shrinks the "inverse" structure approximately 50% in linear dimensions. The fidelity of the process is demonstrated on the macro and micro scale where two halves of the initial stereom, one pyrolyzed (white) and one not (yellow), are shown side by side (Figure 2), along with the smaller scale inverted structure. Using polystyrene (PS) as the second backfilling material enables a *cyclic* size reduction scheme to be realized. The process also allows choice of replicating/reducing either the original or the inverse structure

(Figure 3). After one complete cyclic reduction (two pyrolysis steps), the lattice parameter, *a*, becomes ~ 8 μm. Finally, vacuum-assisted infiltration of the tellurium (Te) into the SiOC network followed by etching the SiOC provided the desired length scale, high dielectric contrast structure having low absorption over a wide range of infrared wavelengths.

Figure 2. SEM images of the native magnesium calcite:air structure (on left) and the inverse pyrolyzed SiOC:air structure (on right). Both views depict the (100) crystal facet. Note that the inverted structure after the pyrolysis step has about a 50% linear decrease in the lattice spacing. The central image depicts a sample cut in half where one half (on right) was pyrolyzed. Note the structural fidelity of the pyrolysis step over the entire sample.

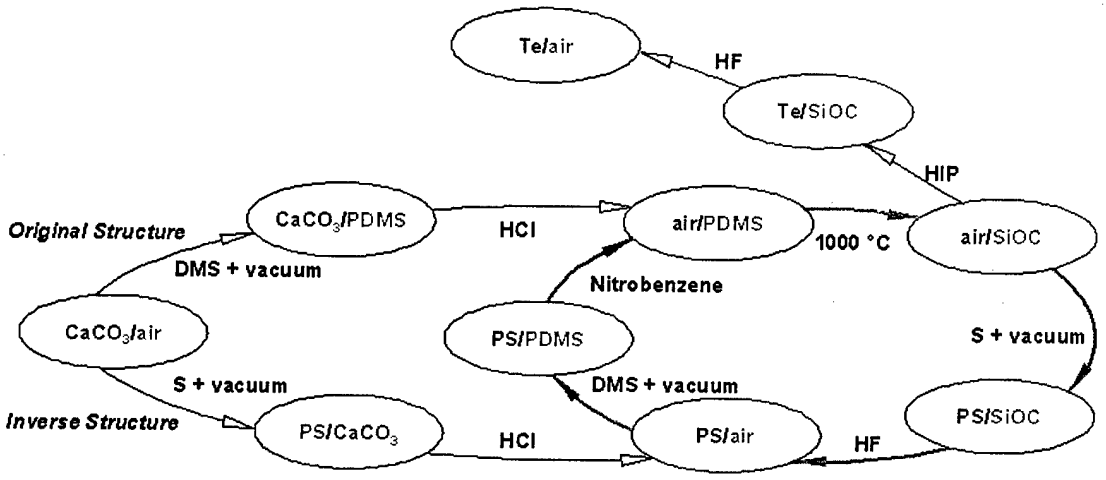

Figure 3. Schematic description of the cyclic size reduction scheme accompanied by a final high dielectric infiltration step. Both the inverse-urchin and direct-urchin structures can be produced depending on the initial infiltration process.

Unpolarized directional reflectance (DR) was used to characterize the mid-IR optical properties of our reduced and infiltrated network. Figure 4 summarizes the room-temperature, near normal (20°) DR spectra, defined as the ratio of the total energy reflected into a

subtending hemisphere to the energy incident on the surface at angle θi_i, from the polished (111) crystal facet of the replica (see inset). A flat film of pure tellurium exhibits a spectrally insensitive reflectance of 46% from 5-40 μm due to the large index with respect to air. A Te:SiOC replica also does not exhibit major spectral features. This is ascribed to the inadequate dielectric contrast between the interpenetrating structures (n_1:n_2 ~ 4.6:2) and the high absorption of SiOC over this spectral region. In contrast, the Te:air replica exhibits a sharp, well defined reflectivity peak centered around 34 μm and a mean reflectance elsewhere approximately half that of a film of pure tellurium (25% versus 46%), corresponding to that expected from a film comprised of the Te:air structure with lower effective index.

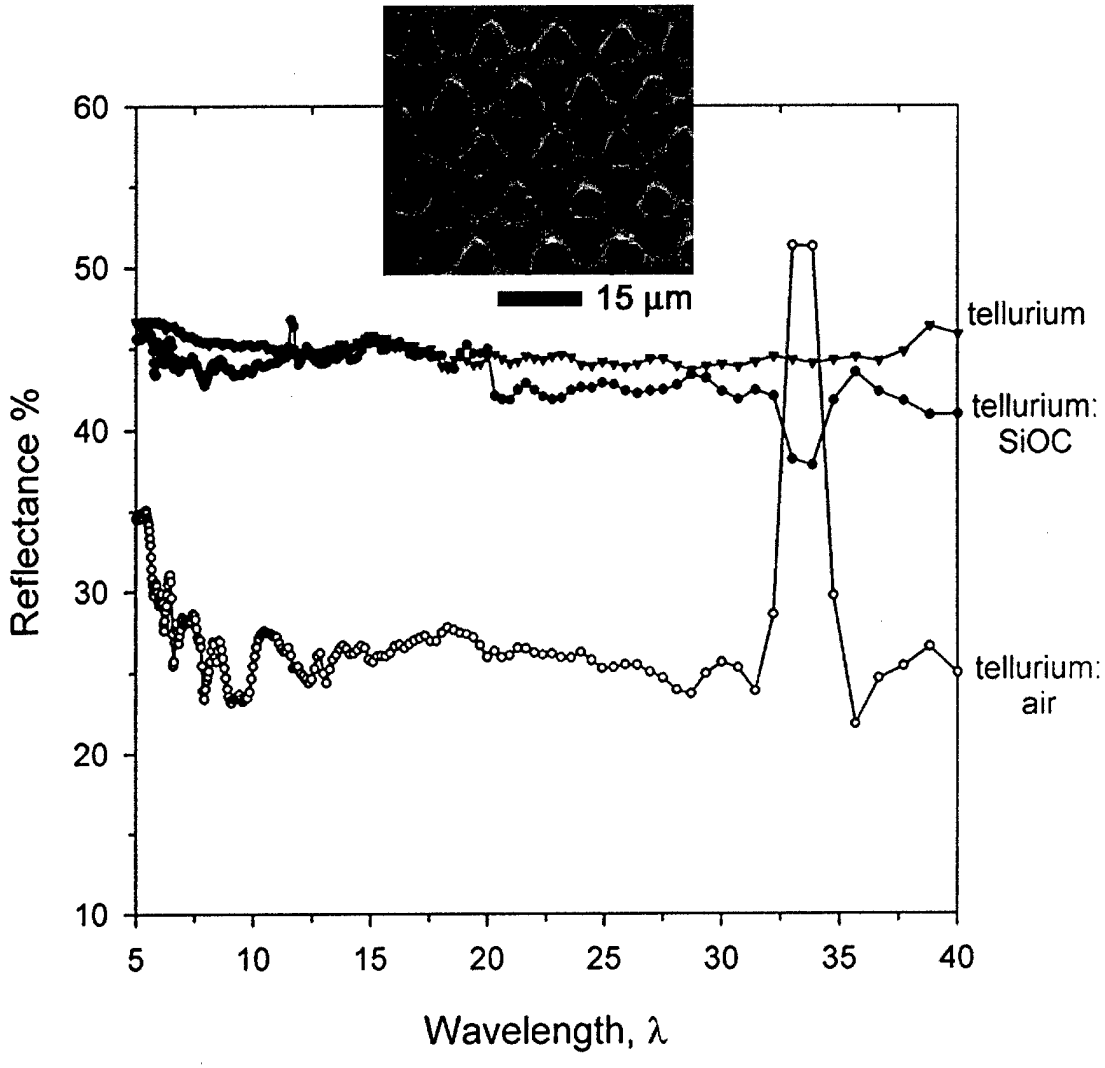

Figure 4. Reflectance spectra at θ_i =20° of the bulk tellurium, tellurium:SiOC and tellurium:air replicas. The inset SEM image shows the three-fold symmetric (111) facet of the tellurium:air network after polishing and etching the tellurium:SiOC structure. The reflectivity peak from tellurium:air, centered at 34 μm, corresponds to the partial bandgap shown in Figure 5.

Based on the calculated band diagram (Te:air refractive index contrast, $n_1:n_2 = 4.6:1$; a = 8μm), the sample should exhibit strong reflectivity between 30 – 36 μm due to the partial gap between the 5^{th} – 6^{th} bands. The measured reflectivity corresponds to the reflection of incident light inclined 20° toward the (110) planes from the (111) facet and corresponds to the gap region located between the R and M points on the band diagram. Both the width and location of the reflectivity notch are consistent with the calculated band diagram shown in Figure 5. Only the dominant stop band appears in the reflectivity data without higher order bands due to the deviation of the sea urchin from a crystallographically perfect structure.

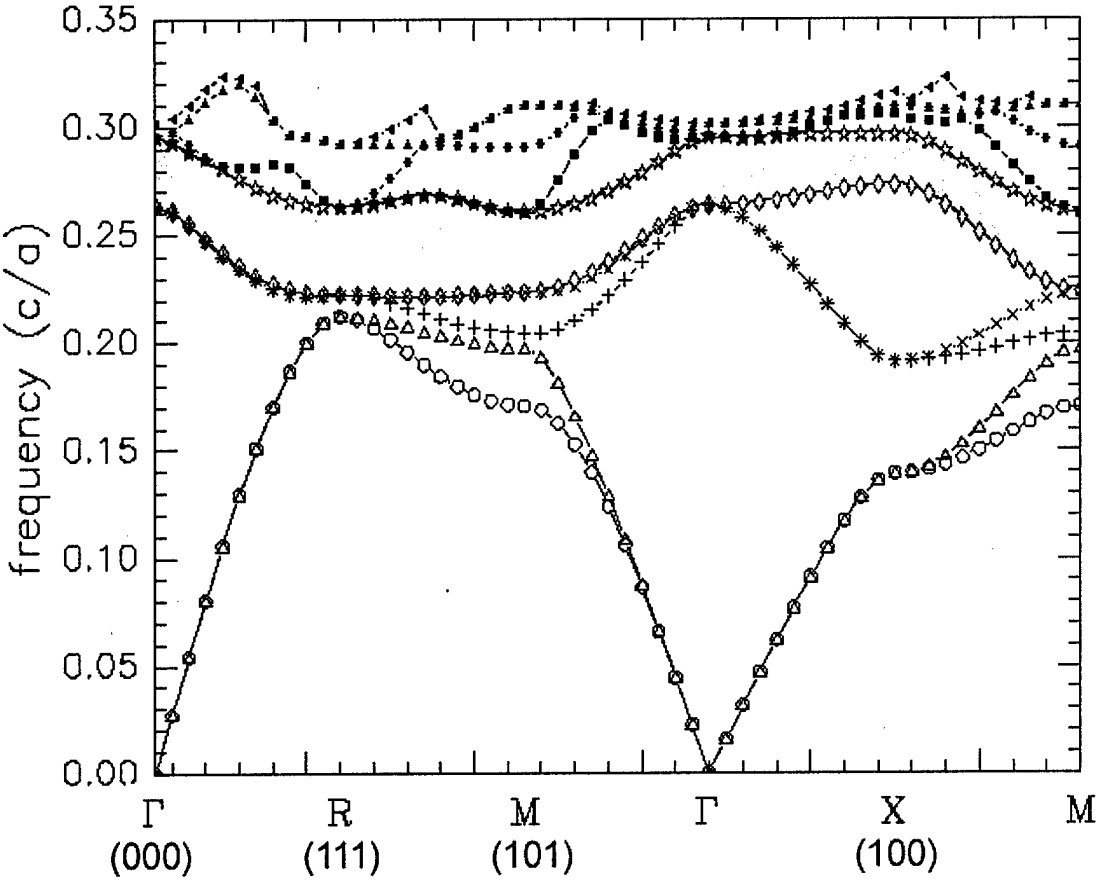

Figure 5. Band structure corresponding to a level set P-surface with 50 vol% structure and a refractive index contrast of $n_1:n_2 = 4.6:1$. A partial bandgap between the 5^{th}-6^{th} bands, as shown in the gray shaded region, occur. Note that previous reports determined a refractive index of the tellurium in the mid and far IR ($\bar{n} = 4.6$) to be less than that reported for elemental tellurium $(\bar{n} = 5.5)$, reflecting incomplete densification and partial oxidation incorporation during processing.

In summary, we have developed a reduction and infiltration process for a naturally occurring 3-D bicontinuous structure to create photonic crystals. The sea urchin exoskeleton can be engineered in a top-down fashion to create low absorption, high dielectric contrast photonic crystals with a stop band in the mid-IR regime. This cyclic reduction-infiltration approach should permit fabrication of a wide variety of 3-D bicontinuous structures based on the many periodic structures exhibited in nature. Details of the experimental procedures and of the cyclic size reduction scheme are included in the Appendix.

Bio-colloids: Bottom-up Engineering of the *Wiseana* Iridescent Virus

Although the assembly of spherical colloids holds promise for generating various periodic 3-D photonic crystals (PCs), spheres may not be the most suitable building blocks for photonic crystals with complete band gaps. The spherical shape and associated spherically symmetric interaction potential facilitates assembly, but also limits potential arrangements to a subset of the cubic space groups, particularly favoring FCC close-packed spheres (opal structure). Additionally, simulations of the 3-D inverse opal structure conclude that size randomness, or polydispersity, of the spherical colloid, has a greater effect in diminishing the breadth of the optical bandgap than site randomness, or distribution, in the lattice dimension. This implies that polydispersity, which usually increases as the size of the particles decrease, has a substantial, detrimental effect on the final optical properties, and is especially critical for higher energy (blue/UV) PC structures. Thus, the exploration of alternate colloidal building blocks with precise shape, size, and surface chemistry may provide new opportunities to form interesting photonic materials.

Viruses offer a number of opportunities that classical colloids do not posses, such as alternative shapes, unique surface chemistry, and monodisperse size. Generically, viruses are comprised of a shell (capsid) consisting of an assembly of 1-3 folded proteins, which surrounds the genetic material (DNA or RNA). Various shapes including helical rods, icosahedra, pleiomorphic enveloped structures and phages with complex tailed morphology, and sizes from about 20 to >300 nm are available depending on the type of virus. Furthermore, by its very nature, the virus particle is monodisperse with highly-defined, symmetrically arrayed variations in particle surface chemistry, which arise from a finite, species-specific number of proteins that fold to create the capsid. The proteinaceous capsid surface provides topological

and chemically distinct sites, which can be engineered to suit specific needs, such as attachment of metal particles.

The present study begins an exploration of the utility of virus particles as component materials for the production of photonic crystals. We investigated the assembly of the insect specific *Wiseana* iridescent virus (WIV) *in vitro*, demonstrating that optical iridescence, much stronger than that commonly observed *in vivo*, can be accessed *in vitro* by various sedimentation or thin film assembly techniques. *In vitro*, the inter-viral interaction potential is characterized by weak long-range electrostatic repulsion and sterically-mediated close-range attraction. The viral assemblies can be readily cross-linked with glutaraldehyde, and exhibit reversible, concentration-dependent optical reflection spectra. Although WIV did not produce non-close packed structures of high perfection, the unique combination of physical and chemical characteristics of viral particles, such as WIV, indicates potential for viruses to complement silica and polymer spheres as a general technology platform for creating optical materials as well as for fundamental studies of soft matter and colloids.

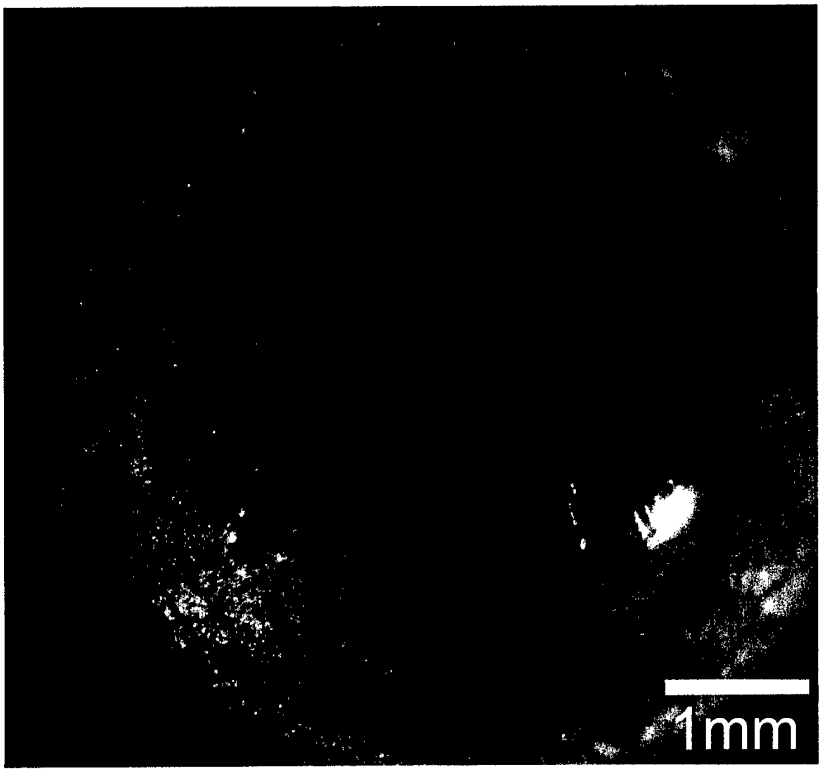

Figure 6. Optical micrograph of glutaraldehyde-fixed WIV pellet assembly, which shows the color gradient produced from a hydration gradient arising from re-swelling of the centrifugate at the pellet – solution interface.

Three assembly methods were investigated: directed sedimentation, sedimentation, and flow-assisted, thin film assembly. The assembly process, and the subsequent structure and associated optical properties reflect the balance of repulsive and attractive forces between the particles and substrate as well as the rate and nature of the forces applied to the particles during assembly. The forces in play between particles include electrostatic (repulsive), steric (repulsive), van der Waals (attractive), and depletion (attractive). Strong short-range attractive potentials typically lead to poorly ordered crystals consisting of a high volume fraction of colloid (>0.5). In these cases, assembly is irreversible, implying that the colloidal lattice cannot be swollen and high quality crystal growth is hampered by the irreversible formation of disordered aggregates. In contrast, weaker short-range attractive interactions lead to reversible colloid association and the ability to re-homogenize agglomerates via swelling of the lattice with a solvent. However, these colloidal crystals are structurally fragile, and require equilibrium with a liquid, such as water, and subsequent cross-linking schemes to increase their rigidity. Longer-range attractive interactions are critical for establishing the initial assembly rates.

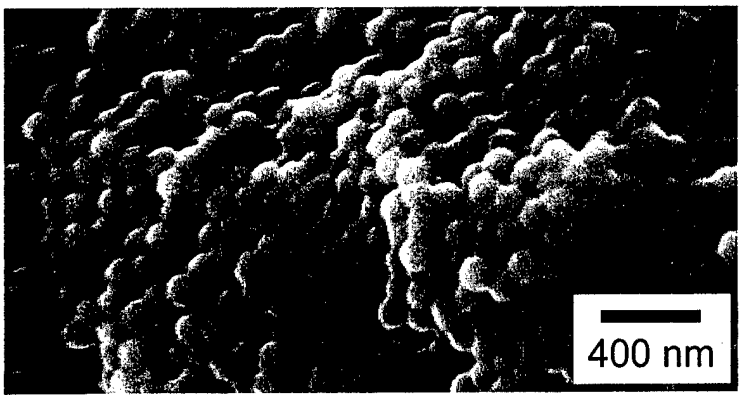

Figure 7. SEM image of glutaraldehyde-fixed WIV pellet showing disordered arrangement of small regions of closed-packed particles. Some individual virus particles show collapsed capsids, from the dehydration of the pellet prior to the application of the 2 nm tungsten coating used for charge dissipation within the SEM.

Directed sedimentation of WIV was performed by centrifugation of 3-8 % solid colloid suspension in water in 1.5 ml vials in a microcentrifuge at 5,600g for 20 min. The subsequent pellets were fixed by extracting the supernatant, immediately adding an aqueous 10% glutaraldehyde solution without disturbing the pellet, and then continuing centrifugation for an additional 20 min. Glutaraldehyde in aqueous form is present as monomeric and polymeric

species containing at least two aldehyde (COH) groups, which form covalent bonds with amines present in the proteins. This cross-links the proteins on the capsid surface and adjacent virus particles. As viewed from the bottom of the centrifugate (Figure 6), the reflected color from the pellet created at 5,6000g varied from blue to red, from the center to the periphery of the pellet. Before cross-linking, these pellets are readily re-suspended by gentle agitation, yielding the same iridescence upon subsequent centrifugation. The color and variation within a pellet was preserved upon cross-linking the structure with glutaraldehyde and persisted after partial dehydration – re-hydration cycles of the cross-linked assembly. The purity of the initial viral suspension impacted the final iridescent color, where bluer iridescence occurred with higher purity viral suspensions prepared with a CsCl gradient, indicating that residual biomacromolecules associate with the viral surface and mediate the closest-packing distance of the particles. The reflection spectra at the center-bottom of the pellet also depended on centrifugation rate, exhibiting a bathochromic shift to green upon decreased centrifugation force (1,400g). More drastic was the variation of reflected color with hydration (see below). The red iridescence near the pellet-solution interface is thought to arise from swelling of the viral assembly upon removal of the centrifugal force at the terminus of fabrication, since the variation in sedimentation force across the pellet (200g) was too small based on assembly experiments at different centrifugation rates (1,000 to 5,600g) to account for the drastic spectral shift. Scanning electron micrographs of numerous fracture surfaces of the *fixed* and *dehydrated* WIV pellet, shown in Figure 7, depict a structure comprised of small regions, ranging from 5-15+ close-packed particles, exhibiting various degrees of local translational order without any orientational correlation to adjacent regions. Figure 8 summarizes the shift of the reflection spectra from the glutaraldehyde cross-linked pellet, assembled at 5,600g, as it dehydrates. The local reflectivity, measured with a Zeiss microscope-spectrophotometer, was collected from the curved face of the fixed pellet. The initial reflectivity was spectrally broad, with a full-width-at-half-maximum (FWHM) of ~100nm, and exhibited a weak low-wavelength shoulder. A 62% reduction in the total mass of the pellet (by water evaporation) decreased the total reflectivity by ~40% and shifted the maximum of the iridescence from 530nm to 480nm. The final spectra of the dehydrated pellet corresponded to the lower wavelength shoulder of the initial hydrated spectra, implying that the initial spectrum was a superposition of interference from a dehydrated surface region and a hydrated bulk.

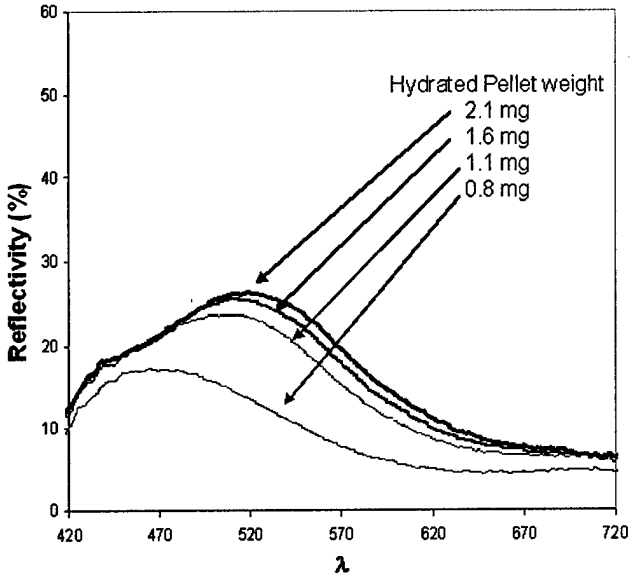

Figure 8. Reflection spectra showing a blue shift towards shorter wavelengths for decreasing water concentrations as the pellet dries out. (lower limit of spectrophotometer ~430nm)

Sedimentation of WIV films was performed between two cleaned and untreated glass slides (cleaned with acetone, isopropyl alcohol, and DI water) sealed on three sides with a 50 μm thick PDMS layer and situated vertically to produce a 3 cm high, 1 cm wide, and 50 μm thick reservoir. A 2-5% virus (or polymer) suspension in water was added to the reservoir and placed in a vacuum dessicator to evacuate air trapped in the reservoir. The sedimentation cells were removed from the vacuum, placed in a refrigerator at 5 ^{0}C, and monitored daily. After two weeks of slow sedimentation, a density gradient of virus particles, from top-to-bottom of the cell, developed. The virus suspension had an opaque grey-blue appearance toward the bottom half of the reservoir, a light cloudy white region toward the top, and an interphase between the two regions showing green/purple iridescence.

Thin film assembly was performed using a cell, which consisted of two glass slides sandwiching a Mylar gasket (25 μm thick). A 2 mm diameter hole was drilled through the center of one glass slide in which a glass tube (5 mm OD, 2 cm long) was affixed with epoxy. Cut glass pieces were cleaned by soaking in KOH for 10 hours and rinsing with DI water. To create a path in the assembled cell large enough for the water to escape but small enough to retain the colloids, the Mylar film was decorated with a small amount of the virus or polymer colloid, by placing it in a .01% suspension of the particles in water for 20 seconds. The

decorated Mylar film was placed on the un-drilled glass slide and a drop of the ~1-2 % solid suspension in water was placed on the slide such that when the top piece of glass with the tubing was placed on the assembly there were no air bubbles trapped in the cell. The cell was held together with two small binder clips. The glass tubing was filled approximately half way with the ~1-2% colloidal suspension, a pipette bulb was placed over the glass tubing to create a slight positive pressure, and the entire assembly was placed on a sonicator for gentle agitation. Once large regions of assembled virus appeared after a few days, the remaining virus solution in the reservoir was replaced with a mixture of 50:50 glutaraldehyde and formaldehyde to fix the assembly and the film was placed on the sonicator for an additional 24 hours. Due to the slow diffusion rate of glutaraldehyde, the 50:50 mixture was used to insure fixation and cross-linking throughout the 25 μm thick iridescent film. Uniform assemblies between glass slides with green iridescence were fabricated. These confined viral films were 5-30 mm in lateral extent and 25 microns (around 100 virus particles) thick. As with the centrifuged pellets, a color change was observed at the lateral periphery of the assembly. A blue-shift at the cell edge is due to evaporation of water that increases viral concentration; whereas a red-shift at the WIV-water interface is due to localized swelling of the growing assembly. Cross-linking the virus assembly did not noticeably change the optical properties of the film. Attempts to remove the film from the assembly cell were unsuccessful, resulting in fracture within the assembly and sections adhering to each side of the cell. Representative morphology of the fracture surface of a dehydrated assembly is shown in Figure 9. After opening the thin film cell, a monolayer of predominately close-packed viral particles adhered to the glass surface. The apparent cracks in the assembly are attributed to volume reduction upon drying. Minimal change in the orientation of the assembly across the fractures implies that before drying the lateral size of the hydrated grains was at least 2-10 microns. The large central portion of the confined, hydrated thin film assembly exhibits an intense, narrow peak (FWHM ~ 25 nm) at normal incidence centered at 560 nm (Figure 10). This is a substantially narrower reflection peak than that observed for pellets prepared by centrifugation (compare with Figure 8) and indicates longer-range correlation and less structural stacking defects in the film. The transmittance notch of the assembly (Figure 11) exhibits a cosine-dependence with viewing angle, consistent with the Bragg interference arising form planes parallel to the sample surface. Since the dried films appear polycrystalline, individual assemblies of close-packed viruses are

either generally oriented with a common symmetry axis perpendicular to the face of the cell, such as [111], or most of the optical interference effects are caused by viral layers closest to the glass surface which are preferentially aligned. As with the pellets, the reflection notch depends on the relative water concentration (interparticle spacing), as seen in Figure 10, shifting approximately 120 nm from the blue-green edge to the red-orange assembly-solution interface. Additionally, the degree of order, reflected by the FWHM, was most extensive for the central region of the assembly, decreasing toward the cell edge and assembly-solution interface. For these cross-linked assemblies, opening the cell underwater resulted in an immediate color change from green to faint red due to the swelling of the now, unconfined film. Removal from the water slowly changed the film from faint red, back to a fainter green, and then to a faint blue/violet as the interparticle separation decreased with water loss. The weaker reflectance corresponded to irreversible creation of defects within the assembly due to the substantial volume changes. When the films are dried, they exhibited a translucent light grey color.

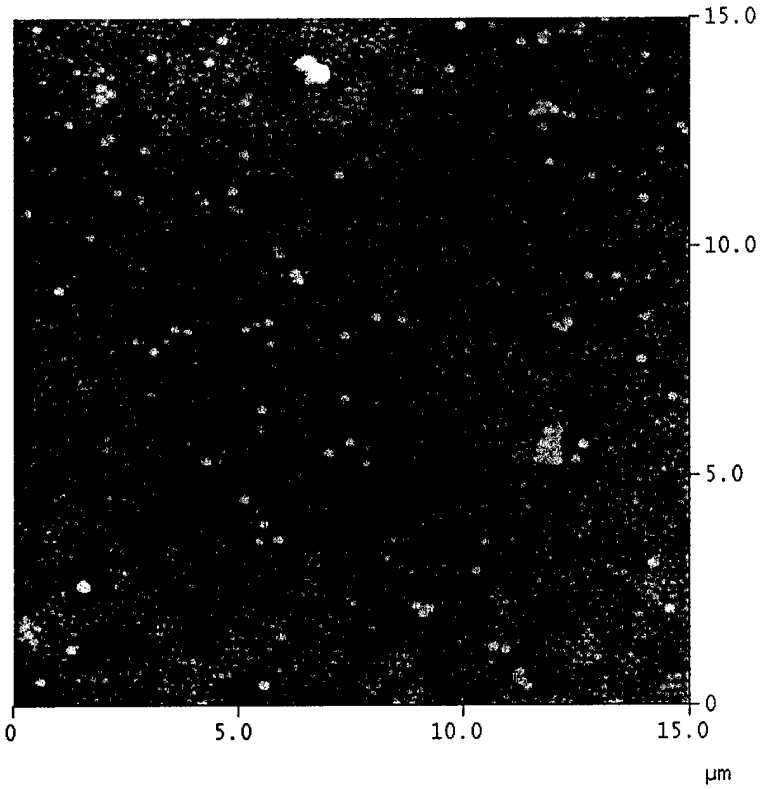

Figure 9. Representative AFM image of polydomain morphology of the WIV assembly toward the center of the film assembly.

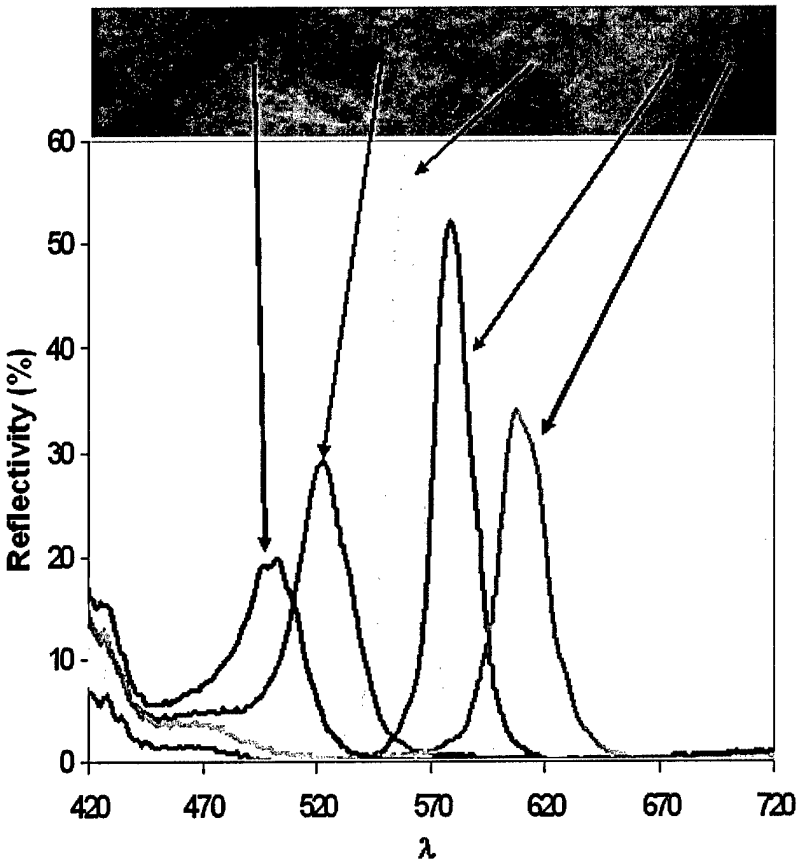

Figure 10. Reflection Spectrum from WIV film created within the confined volume assembly cell at different positions from the cell edge.

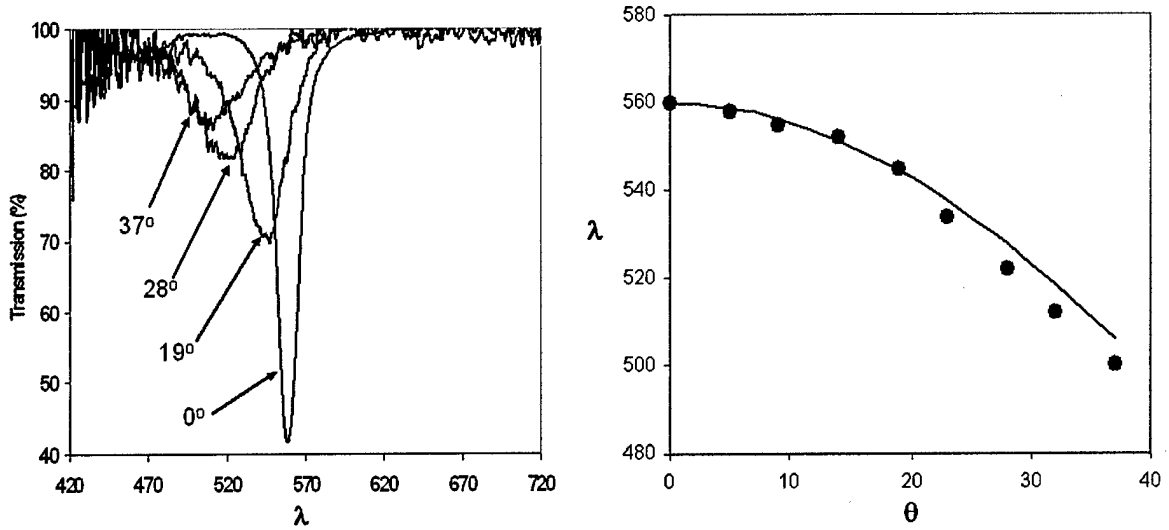

Figure 11. Transmission spectra at varying incident angles showing cosine dependence of transmission notch with tilt angle θ.

In summary, monodisperse viral colloids are a viable building unit to form *in vitro* colloidal assemblies with optical characteristics in the visible spectrum. Both disordered and polycrystalline assemblies occur and exhibit reversible swelling and thus spectral tunability. The photonic crystals were created using three different processing approaches. The optical properties in the centrifuged pellet arise from regions of short-range order as well as from small crystalline regions. Directed techniques, enabling slower assembly, exhibit a more ordered close-packed crystalline morphology. The reflection peak of the assembled viral colloids can be shifted by varying the processing parameters, such as assembly force or by controlling hydration. Details of the experimental procedure are included in the Appendix.

Conclusion

Photonic crystals were constructed using biologically derived building blocks, taking advantage of Nature's ability to efficiently produce highly ordered periodic structures. Both a top-down templating approach and a bottom-up colloidal assembly approach were utilized, and in both instances, processing techniques were developed to successfully make periodic structures with photonic properties in the optical range. In the former case, the bicontinuous periodic exoskeleton structure of the sea urchin was used as a template for a 3-D photonic crystal. A novel cyclic size reduction infiltration/pyrolysis scheme was devised, which could produce high fidelity replicas of the original structure, with a 50% decrease in linear dimensions at each step, and was used to bring the length scale down for optical activity in the mid-IR range (from ~30 μm to ~8 μm). In the latter case, three different processing methods were used to direct the assembly of *Wiseana* iridescent virus particles into ordered colloidal crystals: sedimentation, centrifugation, and flow-assisted assembly. All three methods were successfully used to create photonic crystals in the visible range. The centrifugation and flow-assisted techniques created larger area crystals with better defined spectral properties than the sedimentation technique. Significantly, the spectral properties (color) of the assemblies could be tuned by swelling the cross-linked colloidal crystals with water. This study demonstrated that naturally occurring periodic biological structures could be manipulated into photonic crystal systems, as a first step in creating biologically derived devices for practical engineering applications.

Appendix

Sea Urchin Templating – Experimental Methods

Cyclic reduction. Sylgard 184 from Dow Corning was mixed in a 10:1 monomer:crosslinker ratio and degassed. The sea urchin stereom was then placed in the mixture and the ensemble degassed again which fills the air pores with the PDMS precursor. Polymerization was performed at 60 °C for two hours. The composite was then placed in 10M HCl until all bubble (gaseous CO_2) formation ceased indicating complete etching of $CaCO_3$ ($CaCO_3 + 2HCl \rightarrow H_2O + CO_2 + CaCl_2$). The inverse-urchin PDMS structure is then placed in a tube furnace and the sample is ramped to 1000 °C at 100 °C/hr and held at the temperature for 5 hours, and cooled down to RT at 50 °C/hr. Slow heating and cooling rates ensure minimal to no cracking. The SiOC:air structure was then immersed in styrene monomer (with AIBN as the initiator) and degassed, followed by subsequent polymerization at 100 °C overnight. After polymerization, the sample is heated to 130 °C which softens the PS and allows removal of excess PS on the outside of the sample using tweezers. The SiOC is then etched in HF overnight resulting in a PS:air urchin structure. The air pores are then filled with the PDMS precursor again as discussed above and the PS is dissolved by nitrobenzene – a solvent which dissolves PS but does not swell PDMS. Then the cyclic process can be repeated as desired.

Tellurium infiltration. SiOC:air structure is degassed with tellurium ingots in a hot isostatic press (HIP). The chamber is then heated to 550 °C with 10,000 psi pressure using nitrogen gas which fills in the air pores with the tellurium. The sample is then cooled to room temperature at 50 °C/hr at which point the pressure is released to atmospheric pressure. The sample is then polished at a specific crystallographic orientation and the SiOC is then etched using HF.

Band Diagram Calculation. Bandgap diagrams were calculated using the freely available software package MIT Photonic Bands (MPB) utilizing the equations for the level set P surface family.

Optical Measurements. Directional reflectance was measured using a SOC-100 Hemi-ellipsoidal Reflectometer coupled to a Nicolet Magna-IR™ System 550 Fourier Transform Infrared (FTIR) Spectrophotometer. The light source and the sample are positioned at the foci of an ellipsoidal hemisphere. The optical train, with the exception of the two flat mirrors used to steer the reflected beam into the FTIR, rotates about an axis coinciding with the centre of the sample, providing angular measurements from an incident angle (θ_i defined with respect to the surface normal) from 10° to 80°. The incident datum is calibrated with respect to a standard of known reflectance (gold mirror). The data was obtained in a 'reciprocal' geometry in which the sample was uniformly illuminated with respect to all incident angles by the interior of an ellipsoidal reflector and the scattered radiation collected at $\theta_i = 20°$. Measurements made in this manner are fully equivalent to those utilizing the "direct" mode, in which the source illuminates the sample from a given direction and the radiation scattered by the sample is collected and detected.

Wiseana Iridescent Virus Colloidal Assemblies – Experimental Methods

WIV was grown in infected larvae of the greater waxmoth, *Galleria mellonella.* The infected larvae were maintained on an artificial diet (200 g Farex, 100 g active yeast, 100mg streptomycin sulphate, 80 g honey and 80 g glycerol.) at 20°C in a controlled environment cabinet for 3 weeks. Larvae were collected and homogenized to release the virus particles. The homogenate was filtered through muslin and centrifuged for 5 min at 2,000g in a Beckman JA-14 rotor to remove gross insect contaminants. WIV particles were collected by centrifugation of the resulting clarified supernatant for 30 minutes at 15,000g in a JA-14 rotor. The virus was then centrifuged through a 5-40% w/w sucrose gradient in a Beckman SW32 rotor at 73,000g for 30 minutes. The WIV band was harvested from the gradient, diluted in water, and collected by centrifugation at 25,000g for 30 min in a Beckman JA-20 rotor. The sucrose gradient treatment was repeated to increase viral purity as necessary. Finally, a salt-wash (re-suspended in 1M NaCl, pelleted at 25,000g) was performed to minimize the potential for non-specific surface contamination of the viral particles. Viral particles were resuspended in 10mM Phosphate buffer (pH 7) and 50% glycerol, and stored at $-5\ ^{0}C$ until use. Before any experiments, the virus solutions were centrifuged in a microcentrifuge at 7,000g for 20 min. The supernatant was carefully removed and the viruses were resuspended in 18MΩ Millipore water. The centrifugation, supernatant removal, and re-suspension were repeated three times.

Additional materials used included 10% glutaraldehyde in water and 37% formaldehyde in water (Fluka), 199 nm (± 6 nm) Nanosphere™ size standard polystyrene/polystyrene divinyl benzene copolymer microspheres in water (Duke Scientific Corporation 3000 series), cleaner sonicator, standard microscope glass slides from Fisher, 5 mm OD glass tubing from Fisher, quick setting epoxy, 25 μm thick Mylar films from Dupont Teijin films, and polydimethylsiloxane (PDMS) silicone elastomer Sylgard 184 from Dow Corning.

References

[1] Ha, Y-H., Vaia, R.A., Lynn, W.F., Constantino, J.P., Shin, J., Smith, A.B., Matsudaira, P.T., Thomas, E.L., "3-D Network Photonic Crystal via Cyclic Size Reduction/Infiltration of Sea Urchin Exoskeleton", *Advanced Materials,* **16**, 1091-1094, 2004.

[2] Ullal, C.K., Maldovan, M., Chen, G., Han, Y-J, Yang, S., Thomas, E.L., "Photonic crystals through holographic lithography: simple cubic, diamond-like, and gyroid-like structures", *Applied Physics Letters*, **84**, 5434-5436, 2004.

[3] Shane, B., Juhl, S.B., Chan, E.P., Ha, Y-H., Brunton, J., Ward, V., Dokland, T., Kalmakoff, J., Farmer, B., Thomas, E.L., Vaia, R.A., "Optical Characteristics of *Wiseana* Iridescent Virus Assemblies", *In preparation.*